Progress In Electromagnetics Research, Vol. 137, 311–333, 2013

MEASUREMENT EVALUATION OF THE TGN RADIO CHANNEL MODELS USEFULNESS IN PREDICTING WLAN PERFORMANCE

Kamil Staniec* **and Michal Kowal**

Institute of Telecommunications, Teleinformatics and Acoustics Wroclaw University of Technology, Wroclaw, Poland

Abstract—The purpose of this paper is to discuss the applicability of the TGn radio channel models in estimating the performance of WLAN transmission. The specificity of the indoor radiowave propagation is first discussed, then TGn models are introduced together with a deterministic propagation model created by the authors for predicting the radio channel higher-order parameters. Intensive WLAN measurements have been carried out in two representative propagation environments and compared to theoretical predictions obtained in four configurations: beginning with the original TGN channel models, then enhancing them by including deterministically simulated pathloss and impulse responses and eventually by generating the channel impulse response on a purely random basis. The obtained results should indicate how accurately the general TGn channel models match measurements in real environments and how they compare to proposed successive modifications.

1. INTRODUCTION

The WLAN (Wireless Local Area Network) systems have been present in the customer market since 1997. As the first release, i.e., IEEE 802.11, did not offer impressive performance (i.e., merely 1- and 2 Mb/s of throughput), it was soon replaced with two other offsprings: 802.11b and 802.11a, offering the maximum data rate of up to 11 Mb/s and 54 Mb/s, respectively. In 2003, another WLAN version was released: 802.11g being a 2.4 GHz equivalent in performance to its 802.11a counterpart operating in 5 GHz UNII band. In 2009, a breakthrough 802.11n generation was launched with the maximum

Received 10 January 2013, Accepted 12 February 2013, Scheduled 21 February 2013

* Corresponding author: Kamil Staniec (kamil.staniec@pwr.wroc.pl).

offered throughput of 600 Mb/s due to the use of some innovative techniques such as: MIMO technology (up to 4×4), increased number of subcarriers (now 52 compared to 48 used in previous releases), the channel width (up to 40 MHz versus former 20 MHz) together with enhanced frame-aggregation techniques improving the transmission effectiveness. The market adoption of WLAN systems has lead to a veritable boom in the customers' and vendors' interest which is best expressed in the 30% growth in the Access Points sales per year — a figure maintaining for the past few years. At present, yet another WLAN generation is being strongly promoted, although still in the draft 3.0 stage accepted in May 2012, offering data rates up to 7.2 Gb/s, with the first equipment already available for purchase. Such a momentum could not be left unnoticed by the cellular technologies carriers, vendors as well as scientific communities [1–6]. Owing to its ubiquitous presence at the customers' premises and public institutions, WLAN is now recognized as a serious candidate serving as a technology for offloading the cellular 4th generation LTE (Long Term Evolution) system from a significant amount of the indoor-originated user traffic.

In the sections to follow address the following issues are addressed: in Section 2 some theory behind the multipath radio channel is provided, in Section 3 basic definitions and notations regarding the power delay profile (PDP) are introduced along with a brief survey of available general channel models standardized for nowadays radio systems. In Section 4 the propagation environments, simulators (i.e., one for propagation modeling and the other for the WLAN throughput calculation) and the equipment used in measurements, are overviewed. In Section 5 general WLAN TGn general channel models are presented as well as their modifications proposed by the authors in order to improve the models' sensitivity to site-specific geometry of a given environment. Major conclusions are summarized in Section 7 with a proposal of further research.

2. THE RADIO CHANNEL IN THE MULTIPATH ENVIRONMENT

The analysis of the radio channels as a time-dispersive medium shall start with the observation that the emitted signal will propagate by interacting with the surrounding environment, that involves reflections from objects, transmissions thru obstacles, diffraction on edges and scattering from rough surface. Thus, the signal arriving at the receiver will not come in a single fringe, but as a pack of signals with different amplitudes, phases, angles of arrival, and short time delays, being delayed copies of the original signal [7–16]. Once collected

within a certain time span at a receiver, they sum up in a vector fashion, accounting for their relative phase differences, which causes some copies to overlap constructively if both are in phase or cancel out otherwise. Such a behavior leads to *small-scale fading*, which is a typical propagation effect, especially in the indoor and urban environment. Since the received signal in a multipath channel consists of a series of attenuated, time-delayed, phase-shifted replicas of the transmitted signal, the baseband impulse response of a multipath channel can be given by Equation (1).

$$h(t,\tau) = \sum_{i=0}^{N_{\text{multipath}}-1} a_i(t,\tau) \exp\left[j\left(2\pi f \tau_i(t) + \theta_i(t,\tau)\right)\right] \delta\left(\tau - \tau_i(t)\right) \quad (1)$$

In (1), $h(t, \tau)$ is the radio channel impulse response, $N_{\text{multipath}}$ is the number of multipath components, $a_i(t, \tau)$ and τ_i are the real amplitudes and excess delays, respectively, of i-th component at time t. The phase term $2\pi f\tau_i(t) + \theta_i(t, \tau)$ represents the phase shift due to free space propagation of the i-th component, plus any additional phase shifts which are encountered in the channel. The frequency response $H(f)$ can now be easily obtained from the Fourier transform of $h(t)$. Therefore, since either $h(t)$ or $H(f)$ are needed for an exhaustive characterization of the radio channel, only one of these should be measured (or accurately predicted), while the other one will be obtained by means of the Fourier transform or its inverse. Now, assuming that the signal is transmitted into an AWGN (Additive White Gaussian Noise) radio channel, the output signal will be in the form given by Equation (2), where $x(t)$, $n(t)$ and $y(t)$ represent, respectively, the input signal, the channel white noise and the channel output signal.

$$y(t) = \int_{-\infty}^{\infty} x(\tau)h(t,\tau)d\tau + n(t) \quad (2)$$

It should be noticed that $y(t)$ only represents the channel time response between a single transmitter-receiver pair. If a MIMO

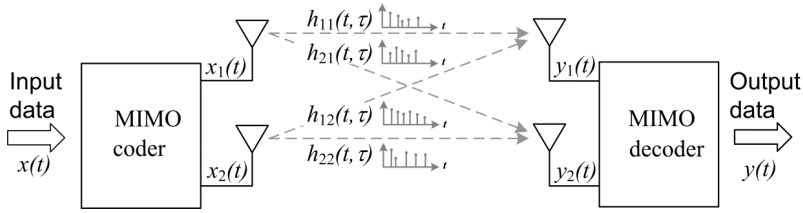

Figure 1. The MIMO configuration in 2×2 antenna set-up.

(Multi-Input Multi-Output) technology is in use, as is the case with IEEE 802.11n devices, say in $M \times N$ configuration (M, N being a number of transmit and receive antennas, respectively), the composite received signal is in fact affected by $M \cdot N$ independent time responses $h_{MN}(t, \tau)$ as shown in Figure 1.

3. THE RADIO CHANNEL POWER DELAY MODELS

Since the multipath power components arrive within some time window, later signal copies (echoes) will tend to posses lower magnitude than the earlier ones. As they come with different time delays, they form a so called power delay profile (PDP) at the receiver, which parameters were explained in [14]. The most crucial of these are: t_{LOS} — the Line-of-Sight propagation time, $t_0 - t_1$ — the time period needed for 95% of the total PDP energy to arrive, enclosed between the peak power and the threshold level P_{th} lying 15 dB lower (see Figure 2(a)). The figure (2(b)) also presents an example PDP obtained in an office environment shown in Figure 5(b), calculated with a deterministic propagation simulator described more exhaustively Section 4.

The issue of the radio channel impulse response has gained considerable importance in the era of broadband digital systems. The reason for this interest can be attributed to the negative effect of the multipath propagation on the received signal quality. Multiple echoes arriving with different (and dynamically changing due to motion) delays and powers are responsible for creating the Inter-

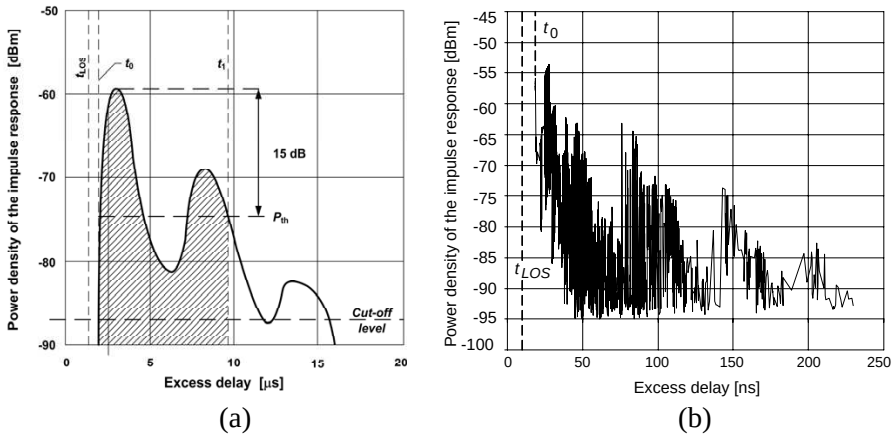

Figure 2. The Power Delay Profile: (a) according to [14]; (b) obtained with the deterministic simulator.

Symbol Interference (ISI) which occurs when delayed versions of a given signal overlap with its earlier copies [15]. For this reason, based on multiple measured PDPs in various environments, general radio channel models have been formulated separately for major digital system and subdivided by the usage scenarios or environments. The systems for which such models have been created include: GSM, WiMAX (IEEE 802.16d/e), UMTS (WCDMA), LTE and WLAN (discussed in a greater detail in Section 5.1); as one can notice, the list spans the majority of systems used in both indoor and outdoor spaces nowadays.

4. ON THE TEST ENVIRONMENTS, SIMULATIONS AND MEASUREMENT SETUP

In the investigations, four elements played a crucial role: 1) two real environments in which measurements were carried out; 2) a WLAN equipment and two simulators — 3) one for obtaining a full information on the radio channel per test point and 4) the other for computing WLAN-OFDM throughput performance, which will now we introduced in this order.

For the purpose of these investigations, a few tens of points ("test points") were selected in two real environments located in Wroclaw University of Technology (building C5, see also Figure 5). At these point simulations of the signal parameters (i.e., the power, delay, angle of arrival — AoA) were carried out to serve as a basis for comparing the estimated throughput versus the measured throughput. The environments were selected so that each is representative to a completely different indoor type: the long corridor provided the 'LOS' case (Line of Sight) conditions where the optical visibility was guaranteed between the transmitter and all test points (20 in total) whereas the suite of offices ('NLOS' case) applied to scenarios with no optical visibility in 83% of cases (46 test points in total).

As regards the radio system for which the reference throughput was measured, two Linksys E4200 access points (in the MIMO 2×2 configuration) were used. They worked in the master-slave mode on the 7th channel (i.e., with the center frequency of 2442 MHz) in the ISM band with the transmit power of 0 dBm and the channel width of 20 MHz. Laptops were located at each end of the connection, running the Iperf software for throughput tests (UDP packets were used for transmission).

The deterministic simulator developed for an exact prediction of the radio signal at selected points is based on the Ray Launching (RL) method [17–22] with the ability to track all multipath components

(up to 2500 in extreme cases) and to log their respective power, delay and AoA in the horizontal and vertical planes. The basic principle consists in discretizing the transmitted wavefront into Q angularly equidistant rays which number is given by (3), where $T \in 1, 2, 3, \ldots$. Such a procedure allows for an easy modeling of the Antenna Radiation Pattern (ARP) as shown in Figure 3(a). Moreover, since individual primary rays tend to diverge from each other as they move away from the source antenna, they can be easily subdivided into secondary rays (Figure 3(b)) to improve the environment scanning resolution (without this mechanism, for instance, some minor objects located far from the

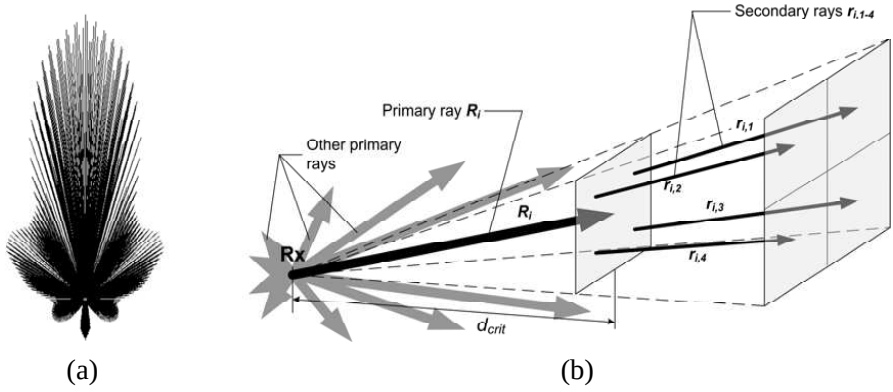

Figure 3. Selected examples of the deterministic RL model: (a) ARP discretization; (b) rays subdivision.

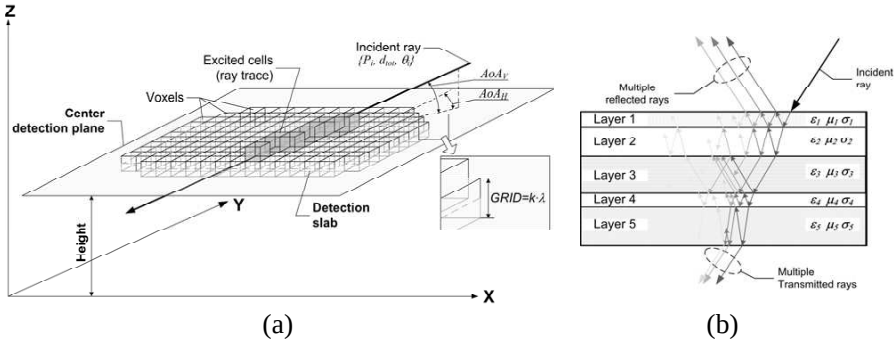

Figure 4. The deterministic RL model operation: (a) the impinging wave traversing through "excited voxels"; (b) the EM wave passing through a multi-layer wall.

source could be omitted).

$$Q(T) = 10 \cdot 4^{T-1} + 2 \tag{3}$$

With the simulator it is possible to track the discrete radio rays (each carrying a proportional part of the total radiated power, multiplied by the directional ARP) propagation inside the environment until a maximum number of interactions has been achieved (set by the authors to 2750 due to the computer memory stack constraints) or until the power of the tracked ray has diminished below a level where its further contribution to the net received power is deemed negligible. An immediate advantage of such an approach can be observed in Figure 4(a) where the received E-field at distinct test points is collected across the entire detection plane with resolution limited to the volume of individual 3D voxels (which size is commonly expressed in terms of the wavelength multiple).

Figure 4(a) demonstrates the information-gathering process in the RL model, where an i-th ray is described by a set of parameters such as: the amplitude (P_i), total distance traveled (d_{tot}), phase (θ_i) and AoA in the vertical and horizontal planes (AoA_V and $\mathrm{Ao}A_H$, respectively). Note that the same set of parameters is recommended for precise time channels analyses of IEEE 802.11x family systems as will be written in depth in Section 5.1.

Beside the above mentioned functionality, the algorithmic engine used in the simulator also allows to consider multi-layer wall structures (see Figure 4(b)), the wave polarization, the presence of objects (e.g., furniture) and persons. Due to its confirmed accuracy of the pathloss predictions with measurements [17, 18], this tool was used to obtain site-specific channel models at each test point in both environments, as an alternative to using environment-general TGn models described in Section 5.1. The simulator will be referred from now on as the "RL simulator" and the pathloss obtained by means of it as the "RL pathloss".

The last component used in the investigations was a software tool created by the authors in Matlab Simulink for simulating the WLAN OFDM (Orthogonal Frequency Division Multiplexing) performance [23]. The entire model consisted of autonomous sub-models: a transmitter, a receiver and a propagation channel for simulating systems compliant with IEEE 802.11g/n standards. During simulations, the available data rates were defined between 6.5 and 540 Mb/s, depending on the selected modulation-coding scheme (MCS), the channel bandwidth B and the propagation fast-fading characteristics in the radio channel. It is noteworthy that with the simulator it was possible to model the transmission directly in the radio band as opposed other analogous simulators capable of emulating

only the baseband operation. This feature made the tool particularly suitable for representing various phenomena occurring in the high-frequency radio channel (such as Rayleigh, Rice fading or AWGN noise) with a great fidelity for comparing the simulated results directly with measurements of real WLAN systems. For an in-depth discussion of the simulator the reader is encouraged to refer to [23, 24].

5. THE WLAN TGN INDOOR RADIO CHANNEL MODEL

There seems to exists a severe drawback in applying general models to represent the time impulse response. The difficulty consists in a great dynamics which characterizes the radio channel time variations measured at even very closely-spaced points. In order to support this assertion, full power delay profiles were found in all test points (as marked in Figure 5) of both environments described in Section 4. Then, for each of these basic points (further on called "reference points" or RP), PDPs was simulated in their direct vicinity, i.e., in auxiliary points (AP) located along rings centered at RP and having the radii of 0.5, 1 and 2-lambda (i.e., the wavelength), containing eight locations in different directions: West (W), North-West (NW) and so forth, as in Figure 6(a). Having calculated the PDPs at all these auxiliary points, they were next compared to the PDP at their respective RP, taking the cross-correlation as a similarity measure. Results averaged over all points in both environments are shown in Figures 6(b)–(c).

In the figure it can be clearly seen that even at points moved merely half a wavelength apart (i.e., between RP and the closest ring

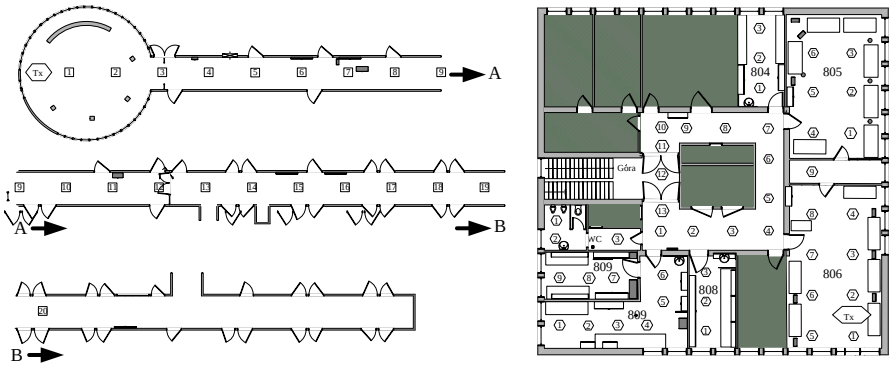

Figure 5. The test environments located at Wroclaw University of Technology: (a) long corridor (112 m); (b) suite of offices (22 × 22 m).

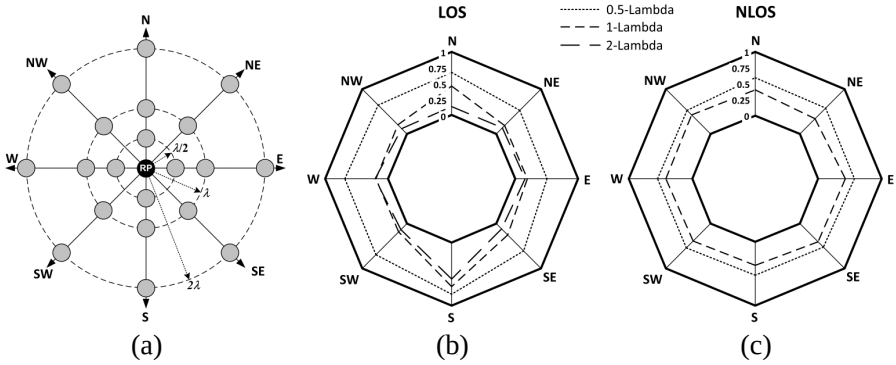

Figure 6. (a) Sets of test points with respect to RPG; signal cross-correlations between locations spaced 0.5, 1 and 2-lambda from RP, under (a) LOS and (b) NLOS conditions.

of surrounding points) the PDP's are correlated at a level close to 0.5. At further distances it decreases down to 0.12 ('LOS' situation, SE direction) at 2λ separation, which in this case equaled 25 cm (see the operating frequency in Section 4). Although only averaged outcomes are presented, the standard deviation never exceeded 0.15 in 'LOS' and 0.16 in 'NLOS' situation, respectively. These results give some idea on how inappropriate it can be to make far-fetched assumptions regarding the relevance of a PDP in a given point in space to PDPs obtained at other points located multiples of wavelengths apart, even in the same indoor environment. Unfortunately, such is the assertion underlying the WLAN TGn models (Section 5.1) which propose a set of universal channel impulse responses supposedly valid for various types of environments.

In the sections to follow respective calculations of WLAN throughput will be performed taking as a basis: firstly — the general TGn channel models, secondly and thirdly — two variants of a detailed channel model obtained from the deterministic simulator, and fourthly — a randomly generated channel. At each step all computations were compared with the measured WLAN 'n' throughput. The purpose for accepting such a procedure was to verify whether or not it is appropriate to apply generic channel models to environments possessing the radio channel variability (dynamics) as great as that encountered indoors.

5.1. The Original WLAN TGn Channel Model

During the work on the IEEE 802.11n technical documentation a set of radio channel models was developed by the TGn (Task Group n) working group (see [25] for details). A description of the channel characteristics has been enhanced with a pathloss model based on a series of measurements both, inside and outside buildings. As a result a set of six distinct channels differing in the impulse response length and the number of clusters, was obtained. Each channel model is representative to some specific environmental conditions, and is distinguished with a letter from the range of A through F. The channel A is not used for the analysis of broadband systems whereas the most commonly utilized models include B, D (shown Figure 7) and E. The impulse response modeling is based on the cluster model [30, 31] and is considered as a tapped delay line with clusters overlapping in the time domain. The power P_{tap} contained in a tap can be found by summing up the powers of all overlapping signal components from all clusters falling into this tap (delay).

Each model is generally composed of two parts: one being the matrix of all channel impulse responses between all M transmit and N receive antennas (according to Figure 1), the other being the pathloss.

The TGn channel models have been elaborated by means of extending the SISO (Single Input Single Output) channel PDPs as

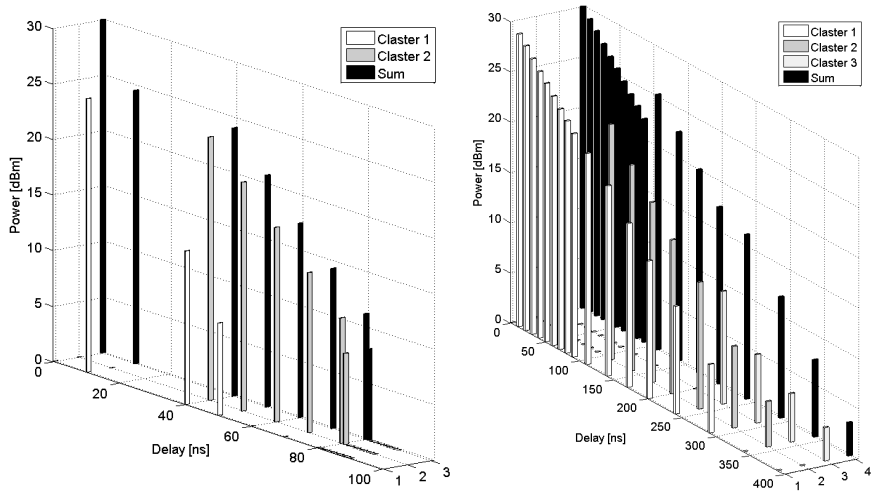

Figure 7. The power delay profile of B and D channel models (the transmit power set to 30 dBm).

in [32] (with a detailed procedure included in [25]) to obtain a resulting channel matrix H defined by Equation (4).

In Equation (4), X is the complex Gaussian variable with zero mean and a unit variance, Φ is the angle of arrival (AoA) or departure (AoD) associated with the LOS component and K is the Rice coefficient. The X variable represents the cross correlation between the transmitting and receiving antenna(s) and can be calculated using the transmitter correlation matrix R_{Tx} and the receiver correlation matrix R_{Rx} by Equation (5).

The elements of R_{Tx} matrix are composite correlation coefficients between the i-th and the j-th transmitting antennas, while the elements of the R_{Rx} matrix are composite correlation coefficients between the i-th and j-th receiving antennas. In the presented channel model complex correlation coefficients are calculated based on PAS (Power Angular Spectrum) which depends on the Angular Spread (AS), AoA in the receiving antenna and AoD in the transmitting antenna. A more detailed calculation procedure can be found in [25].

$$H = \sqrt{P_{tap}} \left(\sqrt{\frac{K}{K+1}} \begin{bmatrix} e^{j\phi_{11}} & e^{j\phi_{12}} & \dots & e^{j\phi_{1M}} \\ e^{j\phi_{21}} & e^{j\phi_{22}} & \dots & e^{j\phi_{2M}} \\ \vdots & \vdots & \ddots & \vdots \\ \rho^{j\phi_{N1}} & \rho^{j\phi_{N2}} & \dots & \rho^{j\phi_{NM}} \end{bmatrix} + \sqrt{\frac{1}{K+1}} \begin{bmatrix} X_{11} & X_{12} & \dots & X_{1M} \\ X_{21} & X_{22} & \dots & X_{2M} \\ \vdots & \vdots & \ddots & \vdots \\ X_{N1} & X_{N2} & \dots & X_{NM} \end{bmatrix} \right) \tag{4}$$

$$[X] = \sqrt{[R_{R_x}]} \left(\left[\hat{X} \right] \sqrt{[R_{T_x}]} \right)^T \tag{5}$$

The TGn pathloss model (or the "TGn pathloss") is described by Equation (6). It distinguishes two distance cases from the transmitter to the receiver, i.e., before and after the breakpoint d_{BP} equal to $2\pi h_{Rx} h_{Tx}/\lambda$ where h_{Rx}, h_{Tx} are the transmit and receive antenna heights in meters, respectively and λ is the wavelength in meters.

$$\begin{aligned} L(d) &= L_{bf}(d) \quad d \le d_{BP} \\ L(d) &= L_{bf}(d) + 35 \log_{10} \left(\frac{d}{d_{BP}} \right) + SF \quad d > d_{BP} \end{aligned} \tag{6}$$

According to the model, when d is shorter than d_{BP}, the total pathloss is equal to that of the free space L_{bf}, given by Equation (7).

$$L_{bf} \left(d_{[\mathrm{m}]}, f_{[\mathrm{MHz}]} \right) = 20 \log_{10}(d) + 20 \log_{10}(f) - 27.55 \text{ [dB]} \tag{7}$$

Table 1. The TGn pathloss model parameters.

Model	d_{BP} (m)	Slope		Shadow fading	
		before d_{BP} [dB]	after d_{BP} [dB]	before d_{BP} [dB]	after d_{BP} [dB]
A	5	2	3.5	3	4
B	5	2	3.5	3	4
C	5	2	3.5	3	5
D	10	2	3.5	3	5
E	20	2	3.5	3	6
F	30	2	3.5	3	6

The breakpoint can be defined as the horizontal distance from the transmitter at which the amplitudes of the direct and reflected waves become nearly identical but having opposite signs. This leads to both waves (i.e., the direct and reflected) cancelling each other. For this reason, for distances smaller than d_{BR} the attenuation slope is 20 dB/decade whereas for distances greater than d_{BR} the attenuation slope is 35 dB/decade. The model can also take into account the shadow fading (SF) coefficient to compensate for the signal fast fading (see also [26–29]). Parameters for the pathloss model are presented in Table 1. The H matrix and the pathloss formula according to the original TGn model specification will be referred to in this paper as the "pure TGn" model.

5.2. The Modified WLAN TGn Channel Model and a Random Channel

For the purpose of investigations, the authors have proposed two modifications to the "pure TGn" model.

The first one, called the "TGn + RL pathloss", consisted in taking only the H matrix from the "pure TGn" model while replacing the original TGn pathloss with the RL pathloss.

In the second one both the H matrix and the pathloss were modified in the following manner: the data obtained from the RL simulator were used to obtain channel models, i.e., $h_{MN}(t, \tau)$, AoA and DoA at each test point in the two propagation environments presented in Section 4. Thus, for each such a point its individual H matrix was created in accordance with Equation (4). The resultant H matrix obtained in this way (or rather a set of H matrices — each corresponding to a different test point) and the RL pathloss will be referred to as "the modified TGn" model from now forth throughout

the paper.

The procedure of creating a PDP with the RL simulator was the following: the value of AS (on both sides of the link) was computed according to the Equation (8) where A is AoA or DoA and P_i is an i-th multipath component power.

$$AS = \sqrt{\frac{\sum_{i=1}^{n} \left(A - \bar{A}\right)^2 P_i}{\sum_{i=1}^{n} P_i}} \tag{8}$$

In the next step the tap powers P_{tap} of all incoming rays were summed up for each of the $M \cdot N$ paths, at every test point. Lastly, the time interval was calculated during which the multipath components contributed to 99% of the total PDP (received) power. The 99%-criterion has been adopted in compliance with the respective recommendation [33] defining the occupied bandwidth B as 99% of the normalized signal power spectrum $W(f)$, as in Equation (9).

$$\int_{-\frac{B}{2}}^{\frac{B}{2}} W(f)d(f) = 0.99 \int_{-\infty}^{\infty} W(f)d(f) \tag{9}$$

It turned out in the simulations that 99% of the entire PDP power was carried by the waves that arrived within the 476 ns and 73 ns time windows for the long corridor and the office, respectively. Hence, for the power delay profiles calculations, only rays with delays not exceeding 480 ns (in the corridor) and 80 ns (in the office), relative to the first recorded ray, were taken into account. Examples of PDPs for points #1 and #10 in both considered environments are presented in Figure 8 and Figure 9.

There was one more modification, called by the authors a "random H". It consisted in running simulations for a randomly generated

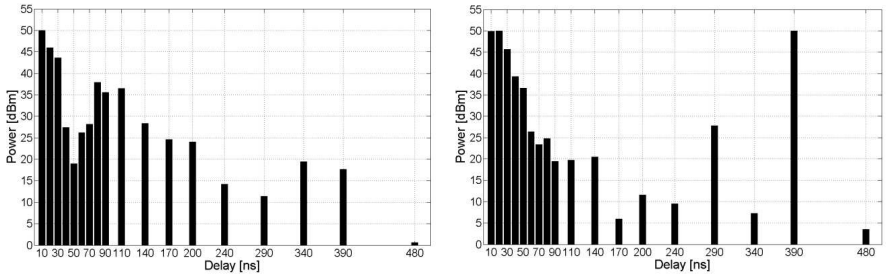

Figure 8. The simulated power delay profile for the modified TGn model in the long corridor (normalized to 50 dBm).

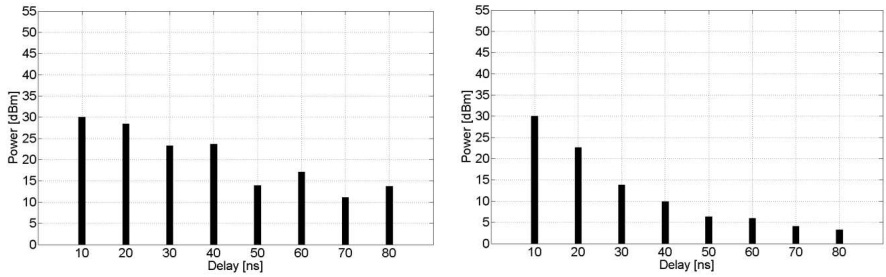

Figure 9. The simulated power delay profile for the modified TGn model in the suite of offices (normalized to 50 dBm).

channel matrix H in the following manner. At first, for each test point 50 random channel matrices were generated with complex normally-distributed elements and the corresponding elements were then averaged. The pathloss was obtained from the RL simulator. Once H was calculated it was used as an input to the MIMO-OFDM simulator which generated outputs in the form of an expected MCS (Table 2) at each test point.

Summarizing, in Sections 6.1–6.2 comparative investigations for both environments were carried out in four scenarios:

- "pure TGn" (see Section 5.1);
- "TGn+RL pathloss" (see Section 5.2);
- "modified TGn" (see Section 5.2);
- "random H" (see Section 5.2).

6. MEASUREMENTS — EVALUATION OF THE RADIO CHANNEL MODELS PERFORMANCE

This chapter presents a comparative analysis of throughput results obtained by simulations and measurements of an IEEE 802.11n-compliant wireless network. In this section a simple way to determine the level of convergence of the simulation and measurement results is proposed. For each scenario an M coefficient was calculated, which was a measure of convergence of the simulated and measured outcomes. The M coefficient is a function of two other factors: M_1 and M_2. The former describes the degree with which trends of simulations and measurements are convergent. Thus it has a meaning of the cross correlation coefficient and assumes values from the range $\langle 0; 1 \rangle$. The closer it approaches a unity, the greater convergence is observed

between both trends. The value of M_2 factor can be interpreted as the average mean relative error, and is given by Equation (10).

$$M_2 = 1 - \frac{1}{n}\sum_{i=1}^{n}\frac{|R_{b_{simulated}}(i) - R_{b_{measured}}(i)|}{R_{b_{measured}}(i)} \tag{10}$$

The value of M_2 coefficient is normalized in the same way as the cross-correlation coefficient and will assume values close to one when the difference between the simulated and the measured throughput is small or tend to zero if the difference is remarkable. Eventually, M coefficient is calculated as an average of M_1 and M_2.

In the simulator radio channel model the Gaussian noise was added to the signal with the noise power in the channel bandwidth B was calculated using Equation (11) where k is the Boltzmann's constant ($1.3806505 \cdot 10^{-23}$ J/K), T_0 is antenna noise temperature (293 K) and F is the noise factor.

$$N = k \cdot T_0 \cdot F \cdot B \tag{11}$$

The complex Additive White Gaussian Noise (AWGN), given by Equation (12), was also added to the signal, with $a_n(t)$ and $b_n(t)$ components being independent real Gaussian variables with zero mean and a standard deviation σ_n. The average noise power P_n of the AWGN can be found from Equation (13).

$$n(t) = a_n(t) + jb_n(t) \tag{12}$$

$$\begin{aligned} P_n &= \frac{E\left[n(t)n^*(t)\right]}{2} = \frac{E\left[\left(a_n(t) + jb_n(t)\right)\left(a_n(t) - jb_n(t)\right)\right]}{2} \\ &= \frac{E\left[a^2(t)\right] + E\left[b^2(t)\right]}{2} = \frac{\sigma_n^2 + \sigma_n^2}{2} = \sigma_n^2 \end{aligned} \tag{13}$$

All the above considerations have led us to the formula for the Signal to Noise Ratio at the receiver input, defined by Equation (14) where A_m^2 is the $y(t)$ signal amplitude. SNR is a basic metric of the received signal quality which serves as basic parameter for a device to decide on the choice of a particular MCS. Due to the channel temporal variations, the received signal power S is subject to short-time changes and its value is used by the receiver to adapt its transmission rate determined by a respective MCS, depending on conditions in propagation channel (see Table 2). The noise power P_n is here obtained from Equation (13).

$$\text{SNR} = \frac{\text{Signal power}, S}{\text{Noise power}, P_n} = \frac{A_m^2 E\left[y^2(t)\right]}{2P_n} = \frac{A_m^2 E\left[y^2(t)\right]}{2\sigma_n^2} \tag{14}$$

Table 2. Receiver minimum input level sensitivity of IEEE 802.11n.

Modulation-Coding Scheme (MCS)		**Minimum signal power, S [dBm]**	
Modulation	**Coding Rate**	**Channel bandwidth $B = 20$ MHz**	**Channel bandwidth $B = 40$ MHz**
BPSK	1/2	−82	−79
QPSK	1/2	−79	−76
QPSK	3/4	−77	−74
16-QAM	1/2	−74	−71
16-QAM	3/4	−70	−67
64-QAM	2/3	−66	−63
64-QAM	3/4	−65	−62
64-QAM	5/6	−64	−61

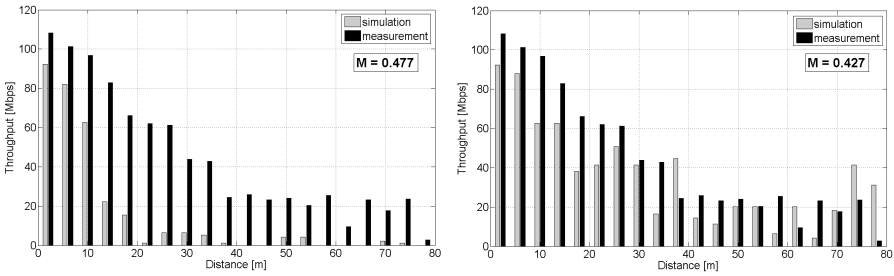

Figure 10. Simulations vs. measurements for the long corridor: (a) the "pure TGn" channel model; (b) the "TGn + RL" pathloss.

6.1. Simulations vs. Measurements in the Long Corridor

In the long corridor the simulations were carried out for packets of 7350 bytes in length (i.e., by aggregating five 1470 B frames in a single one). This value was chosen experimentally as one giving the closest agreement between the simulated and the measured results under interference-free conditions. The maximum tolerable bit error rate was set to 0.1%.

In Figure 10(a) simulations were carried out for the original TGn channel model. Both, the channel matrix and pathloss were calculated

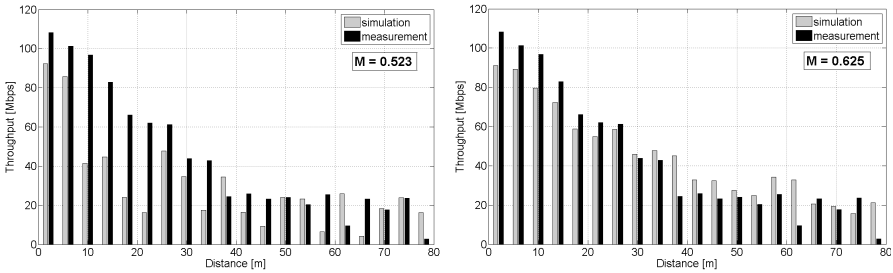

Figure 11. Simulations vs. measurement for a long corridor: (a) the "modified TGn" channel model; (b) the "random H" case.

in accordance with the procedure described in Section 5.1. Although the convergence turned out to be relatively high ($M = 0.477$), the simulated throughput lied far below that measured due to the fairly large pathloss returned by the TGn pathloss model. This considerable pathloss was associated with the fact, that in TGn pathloss model the breakpoint distance d_{BP} is constant (for the TGn channel 'D' equal to 10 m) therefore the simulated signal quickly entered the 35 dB/decade region. On the right of Figure 10 simulated results using the TGn channel are presented with the TGn pathloss now replaced with a median pathloss obtained from the RL model. Although the resultant M coefficient was only 0.427 in this case, the simulated throughput now seems to match the measured one more closely. The average mismatch between simulations and measurements in the "pure TGn" channel scenario was 28.94 Mb/s (Figure 10(a)) whereas for the other (i.e., with RL pathloss) scenario it equaled 11.03 Mb/s (Figure 10(b)). Such results indicate that the M coefficient apparently favors the convergence of trends (higher for the "pure TGn" channel simulations) than the accuracy in the absolute values of the predicted factor (throughput here).

As regards the "modified TGn" model, since it was formulated on the basis of accurate environment-specific measurements and simulations of PDP and pathloss, quite expectedly an improvement in M (now equal to 0.523) was observed, as presented in Figure 11(a). Quite surprisingly, however, the highest M coefficient of all so far was achieved in the "random H" scenario, shown in Figure 11(b), with $M = 0.625$ compared to $M = 0.477$ in the "pure TGn" channel (Figure 10(a)), indicating the greatest convergence between the measurement and simulation results.

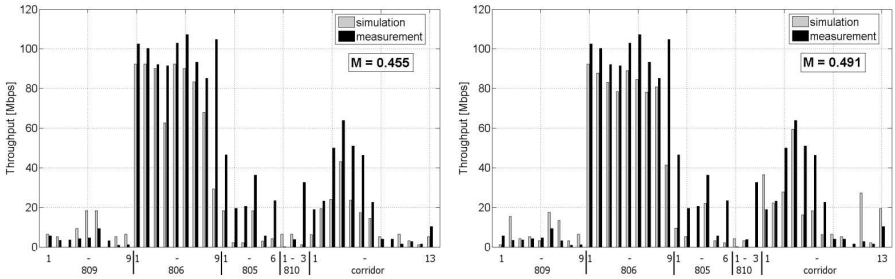

Figure 12. Simulations vs. measurements for the suite of offices: (a) the "pure TGn" channel model; (b) the "TGn + RL" pathloss.

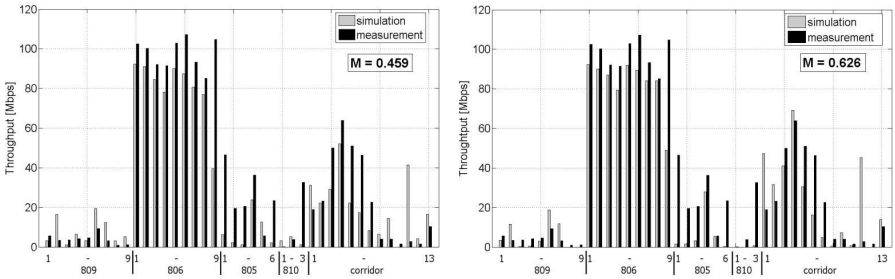

Figure 13. Simulations vs. measurement for the suite of offices: (a) the "modified TGn" channel model; (b) the "random H" case.

6.2. Simulations vs. Measurements in the Suite of Offices

Investigations analogous to those presented in Section 6.1 were performed also for the suite of offices in which the radiowave propagated mainly due to multiple reflections and transmissions through walls rather than to the waveguiding effect as was the case in the long corridor.

As one can notice in Figure 12 the simulated results were by and large lower compared to those measured, with the M coefficient at 0.455 in the (a) "pure TGn model" and 0.491 in the (b) "TGn + RL pathloss" case. In the "modified TGn" scenario (Figure 13(a)), although this environment-specific approach indeed brought about some minor improvement (i.e., $M = 0.459$) over the "pure TGn" version, it performed worse than in the "TGn + RL pathloss" case

Table 3. A summary of the M coefficient values for all four tested configurations.

The H matrix + pathloss scenario	**The long corridor**	**The suite of offices**
a) "Pure TGn" (see Section 5.1)	0.477	0.455
b) "TGn + RL pathloss" (see see Section 5.2)	0.427	0.491
c) "Modified TGn" (see see Section 5.2)	0.523	0.459
d) "Random H" (see see Section 5.2)	**0.625**	**0.626**

($M = 0.491$). Finally, for the "H matrix" case the M coefficient was 0.626 in Figure 13(b).

Again, like with the long corridor results presented in the previous section, the agreement between predictions and measurements kept increasing as we progressed with the radio channel in its "pure TGn" form ($M = 0.455$) through the addition a deterministically calculated pathloss up to a completely random H matrix elements selection ($M = 0.626$).

7. CONCLUSIONS

The chief purpose of the article was to verify the performance of the WLAN TGn channel models for predicting throughput in real-life scenarios. For this reason, two environments possessing very different geometry were selected and digitized with a great degree of precision. Then, throughput measurements were carried out in a few tens of known locations (test points) between a pair of IEEE 802.11n routers — these results now served as a reference for throughput predictions. For the throughput calculations such four cases were then considered: a) the TGn radio channel and the pathloss obtained from its native propagation model, b) the TGn radio channel and the pathloss obtained with the RL model, c) the modified TGn channel model and the pathloss obtained with the RL model, d) the randomly-generated channel model and the pathloss obtained with the RL model. Accepting the convergence coefficient Mas a basic metric for finding the correlation between the reference measurements and the calculated throughput in each of the a)–d) scenarios, results clearly indicate (see also Table 3) that the general TGn models definitely over-generalize the radio channel and lead to the least accurate predictions in all cases.

As a justification supporting these results an explanation was provided in Section 5 where the authors demonstrate that the radio signals received in points spaced by a single wavelength are almost

completely decorrelated while increasing this separation leads to the correlation dropping down to virtually zero (which is a rather well-known fact, verified here by means of simulations). It explains why considering a single channel model fit for all indoors of a certain kind may cause significant errors when compared to measurements. In the "modified TGn" channel, the authors performed simulations on the digitized versions of both test environments with the use of an RL simulator and extracted an averaged channel model from the modeled test points. The two general (modified) models obtained in this way matched the characteristics of the particular environments much closer than their original TGn counterparts. As turned out, this procedure did improve the convergence between the predictions and measurements. However, most interestingly the highest correlation was found when the channel matrix was generated randomly and the pathloss was obtained with the deterministic simulator using digitized maps of the two environments. This configuration is also the authors' recommended one for successful throughput calculation of WLAN transmission. Not only does absolve the WLAN designer from the knowledge of the TGn models and the need to decide which of them most correctly corresponds to the specific environment, but it also expedites the whole prediction process by simply generating a random H matrix and using a site-specific pathloss

REFERENCES

1. Chu, J.-H., K.-T. Feng, and C.-C. Liao, "Analysis and determination of cooperative MAC strategies from throughput perspectives," *Wireless Networks*, Dec. 2012, DOI 10.1007/s11276-012-0529-x.
2. Yu, X., L. Wang, H.-G. Wang, X. Wu, and Y.-H. Shang, "A novel multiport matching method for maximum capacity of an indoor MIMO system," *Progress In Electromagnetics Research*, Vol. 130, 67–84, 2012.
3. Pauliukas, D. and V. Vosylius, "Research of real time traffic transmission in 802.11 WLANs," *Elektronika ir Elektrotechnika*, Vol. 7, No. 95, 111–114, 2009.
4. Kajackas, A. and L. Pavilanskas, "Analysis of the technological expenditures of common WLAN models," *Elektronika ir Elektrotechnika*, Vol. 8, No. 72, 19–24, 2006.
5. Wei, K., Z. Zhang, and Z. Feng, "Design of a dualband omnidirectional planar microstrip antenna array," *Progress In Electromagnetics Research*, Vol. 126, 101–120, 2012.

6. Deruyck. M., W. Vereecken, W. Joseph, B. Lannoo, M. Pickavet, and L. Martens, "Reducing the power consumption in wireless access networks: Overview and recommendations," *Progress In Electromagnetics Research*, Vol. 132, 255–274, 2012.
7. Alsehaili, M., "Angle and time of arrival statistics of a three dimensional geometrical scattering channel model for indoor and outdoor propagation environments," *Progress In Electromagnetics Research*, Vol. 109, 191–209, 2010.
8. Phaebua, K., C. Phongcharoenpanich, M. Krairiksh, and T. Lertwiriyaprapa, "Path-loss prediction of radio wave propagation in an orchard by using modified UTD method," *Progress In Electromagnetics Research*, Vol. 128, 347–363, 2012.
9. Ndzi, D. L., M. A. M. Arif, A. Y. M. Shakaff, M. N. Ahmad, A. Harun, L. M. Kamarudin, A. Zakaria, M. F. Ramli, and M. S. Razalli, "Signal propagation analysis for low data rate wireless sensor network applications in sport grounds and on roads," *Progress In Electromagnetics Research*, Vol. 125, 1–19, 2012.
10. Yu, X., L. Wang, H.-G. Wang, X. Wu, and Y.-H. Shang, "A novel multiport matching method for maximum capacity of an indoor MIMO system," *Progress In Electromagnetics Research*, Vol. 130, 67–84, 2012.
11. Chen, Z. and Y.-P. Zhang, "Effects of antennas and propagation channels on synchronization performance of a pulse-based ultra-wideband radio system," *Progress In Electromagnetics Research*, Vol. 115, 95–112, 2011.
12. Ndzi, D. L., K. Stuart, S. Toautachone, B. Vuksanovic, and D. Sanders, "Wideband sounder for dynamic and static wireless channel characterisation: Urban picocell channel model," *Progress In Electromagnetics Research*, Vol. 113, 285–312, 2011.
13. ITU, ITU-R P.1145, "Propagation data for the terrestrial land mobile service in the VHF and UHF bands," 1995.
14. ITU, ITU-R P.1407, "Multipath propagation and parameterization of its characteristics," 2009.
15. Rappaport, T. S., *Wireless Communications. Principles and Practice,* 2nd Edition, Prentice Hall, 2002.
16. Hashemi, H., "The indoor radio propagation channel," *IEEE Proceedings*, Vol. 81, No. 7, 943–968, Jul. 1993.
17. Staniec, K., "The indoor radiowave propagation modeling in ISM bands for broadband wireless systems," Ph.D. Dissertation, Wroclaw University of Technology, Wroclaw, Poland, 2006.

18. Pomianek, A. J., K. Staniec, and Z. Jóskiewicz, "Practical remarks on measurement and simulation methods to emulate the wireless channel in the reverberation chamber," *Progress In Electromagnetics Research*, Vol. 105, 49–69, 2010.
19. Staniec, K. and A. J. Pomianek, "On simulating the radio signal propagation in the reverberation chamber with the ray launching method," *Progress In Electromagnetics Research B*, Vol. 27, 83–99, 2011.
20. Reza, A. W., M. S. Sarker, and K. Dimyati, "A novel integrated mathematical approach of ray-tracing and genetic algorithm for optimizing indoor wireless coverage," *Progress In Electromagnetics Research*, Vol. 110, 147–162, 2010.
21. Liu, Z.-Y. and L.-X. Guo, "A quasi three-dimensional ray tracing method based on the virtual source tree in urban microcellular environments," *Progress In Electromagnetics Research*, Vol. 118, 397–414, 2011.
22. Sarker, M. S., A. W. Reza, and K. Dimyati, "A novel ray-tracing technique for indoor radio signal prediction," *Journal of Electromagnetic Waves and Applications*, Vol. 25, Nos. 8–9, 1179–1190, 2011.
23. Kowal, M., "The performance of the MIMO-OFDM radio interface in presence of interferences," Ph.D. dissertation, Wroclaw University of Technology, Wroclaw, Poland, 2011.
24. Kowal, M., S. Kubal, P. Piotrowski, and R. Zieliński, "A simulation model of the radio frequency MIMO-OFDM system," *International Journal of Electronics and Telecommunications*, Vol. 57, No. 3, 323–328, 2011.
25. Erceg, V., L. Schumacher, and P. Kyritsi, "TGn channel models," IEEE 802.11-03/940r4, May 10, 2004.
26. Kara, A., "Human body shadowing variability in short range indoor radio links at 3–11 GHz," *Int. Journal of Electronics*, Vol. 96, 205–211, 2009.
27. Cotton, S. L., et al., "An experimental study on the impact of human body shadowing in off-body communications channels at 2.45 GHz," *Proc. 5th European Conference on Antennas and Propagation (EUCAP)*, 3133–3137, 2011.
28. Cheffena, M., "Physical-statistical channel model for signal effect by moving human bodies," *EURASIP Journal on Wireless Communications and Networking*, Vol. 2012, 77, 2012.
29. Kara, A. and E. Yazgan, "Modelling of shadowing loss for huge non-polygonal structures in urban radio propagation," *Progress*

In Electromagnetic Research B, Vol. 6, 123–134, 2008.

30. Li, Q., M. Ho, V. Erceg, A. Jangganntham, and N. Tal, "802.11n channel model validation," IEEE 802.11-03/894r1, Nov. 2003.
31. Saleh, A. A. M. and R. A. Valenzuela, "A statistical model for indoor multipath propagation," *IEEE Journal of Selected Areas in Communications*, Vol. 5, 128–137, 1987.
32. Medbo, J. and P. Schramm, "Channel models for HIPERLAN/2," ETSI/BRAN Document No. 3ERI085B, 1998.
33. ITU, ITU-R F.1191-3, "Necessary and occupied bandwidths and unwanted emissions of digital fixed service systems," May 2011.